

PHOTOGRAPH THIS SHEET

AD A O 78862

DTIC ACCESSION NUMBER



LEVEL



INVENTORY

"Fractographic Analysis of Optical Fibers"

DOCUMENT IDENTIFICATION

Nov. '77

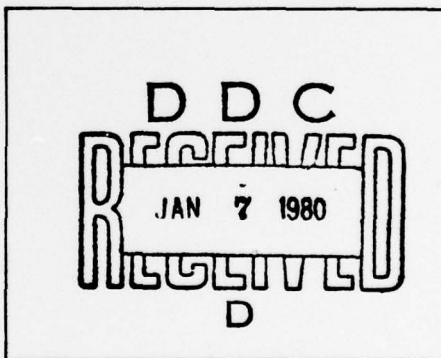
DISTRIBUTION STATEMENT A

Approved for public release;
Distribution Unlimited

DISTRIBUTION STATEMENT

ACCESSION FOR	
NTIS	GRA&I <input checked="" type="checkbox"/>
DTIC	TAB <input type="checkbox"/>
UNANNOUNCED	<input type="checkbox"/>
JUSTIFICATION	
BY	
DISTRIBUTION /	
AVAILABILITY CODES	
DIST	AVAIL AND/OR SPECIAL
A	

DISTRIBUTION STAMP



DATE ACCESSIONED

79 12 3 147

DATE RECEIVED IN DTIC

PHOTOGRAPH THIS SHEET AND RETURN TO DTIC-DDA-2

AD A078862

FRACTOGRAPHIC ANALYSIS OF OPTICAL FIBERS

by

J.J. Mecholsky, S.W. Freiman and S.M. Morey
Naval Research Laboratory
Washington, D.C. 20375

APPROVED FOR PUBLIC RELEASE
DISTRIBUTION UNLIMITED

Prepared for
Defense Advanced Research Projects Agency
ARPA Order No. 3285

November 1977

Interim Technical Report 1

18

Unclassified

SECURITY CLASSIFICATION OF THIS PAGE (When Data Entered)

REPORT DOCUMENTATION PAGE		READ INSTRUCTIONS BEFORE COMPLETING FORM
1. REPORT NUMBER	2. GOVT ACCESSION NO.	3. RECIPIENT'S CATALOG NUMBER
4. TITLE (and Subtitle) Fractographic Analysis of Optical Fibers		5. TYPE OF REPORT & PERIOD COVERED Interim Technical Report 1
7. AUTHOR(s) Mecholsky, J. J., Freiman, S. W., and Morey, S. M.		6. PERFORMING ORG. REPORT NUMBER NRL 533 876
9. PERFORMING ORGANIZATION NAME AND ADDRESS Naval Research Laboratory Washington, D.C. 20375		8. CONTRACT OR GRANT NUMBER(s) DARPA Order 3285
11. CONTROLLING OFFICE NAME AND ADDRESS DARPA/MSO 1400 Wilson Boulevard Arlington, VA 22209		10. PROGRAM ELEMENT, PROJECT, TASK AREA & WORK UNIT NUMBERS 63M05-10
14. MONITORING AGENCY NAME & ADDRESS (if different from Controlling Office) Naval Oceanographic Systems Command San Diego, CA 92152		12. REPORT DATE November 1977
		13. NUMBER OF PAGES 32
		15. SECURITY CLASS. (of this report) Unclassified
16. DISTRIBUTION STATEMENT (of this Report) APPROVED FOR PUBLIC RELEASE DISTRIBUTION UNLIMITED		15a. DECLASSIFICATION/DOWNGRADING SCHEDULE
17. DISTRIBUTION STATEMENT (of the abstract entered in Block 20, if different from Report)		
18. SUPPLEMENTARY NOTES		
19. KEY WORDS (Continue on reverse side if necessary and identify by block number) Glass fracture Communications Fractography Failure Analysis Fiber strength		
20. ABSTRACT (Continue on reverse side if necessary and identify by block number) The fracture surfaces of over 50 fibers tested at Hughes or ITT Research Laboratories were examined on the scanning electron microscope (SEM). The sources of failure in these fibers were determined to be either mechanically induced sharp cracks, cracks resulting from inclusions or foreign particles, bubbles or in- clusions. It was suggested that many of these sources of failure can be eliminated by changing production procedures. For example,		

DD FORM 1473
1 JAN 73

EDITION OF 1 NOV 68 IS OBSOLETE
S/N 0102-014-6601

Unclassified

SECURITY CLASSIFICATION OF THIS PAGE (When Data Entered)

Unclassified

SECURITY CLASSIFICATION OF THIS PAGE(When Data Entered)

some larger inclusions can be eliminated by using synthetic, high grade silica, starting material. Another example for eliminating low strength defects is by using high quality silica tubing in the CVD process.

The fracture surface demarcations known in glass as mirror, mist, hackle, and crack branching were identified and related to the stress, σ , at failure:

$$\sigma r_i^{\frac{1}{2}} = \text{constant} = A_i$$

where r_i is either the mirror-mist, mist-hackle or crack branching boundary corresponding to a different constant, A_i . In all cases but one fracture surface analysis agreed with measured stresses during testing within experimental accuracy. Thus, fractography can be used to determine the stress and source of unexpected service failures.

Unclassified

SECURITY CLASSIFICATION OF THIS PAGE(When Data Entered)

Fractographic Analysis of Optical Fibers

J.J. Mecholsky, S.W. Freiman and S.M. Morey
Naval Research Laboratory
Washington, D.C. 20375

ABSTRACT

The fracture surfaces of over 50 fibers tested at Hughes or ITT Research Laboratories were examined on the scanning electron microscope (SEM). The sources of failure in these fibers were determined to be either mechanically induced sharp cracks, cracks resulting from inclusions or foreign particles, bubbles or inclusions. It was suggested that many of these sources of failure can be eliminated by changing production procedures. For example, some larger inclusions can be eliminated by using synthetic, high grade silica, starting material. Another example for eliminating low strength defects is by using high quality silica tubing in the CVD process.

The fracture surface demarcations known in glass as mirror, mist, hackle and crack branching were identified and related to the stress, σ , at failure:

$$\sigma r_i^{\frac{1}{2}} = \text{constant} = A_i$$

where r_i is either the mirror-mist, mist-hackle or crack branching boundary corresponding to a different constant, A_i . In all cases but one fracture surface analysis agreed with measured stresses during testing within experimental accuracy. Thus, fractography can be used to determine the stress and source of unexpected service failures.

FRACTOGRAPHIC ANALYSIS OF OPTICAL FIBERS*

J.J. Mecholsky, S.W. Freiman and S.M. Morey
Naval Research Laboratory
Washington, D.C. 20375

INTRODUCTION

There is increasing interest in optical glass fibers as a means of communication throughout DoD. Many applications, however, require that the fibers be subjected to stresses in the 100-200,000 psi range for long periods of time. It is therefore important that the fibers be as flaw free as possible. Fractographic analysis is an extremely useful technique for identifying the source of failure as well as for determining the stresses and/or the time to failure of a particular fiber.

Several sets of fibers have been sent to the Naval Research Laboratory from Hughes Research Laboratories, ITT Laboratories and from ITT through NOSC after testing. As will be shown, in many cases the failure source can be related to problems in the manufacture of the preform or in the drawing process itself. Because the low strength tail in strength distribution is the controlling factor in the strength of long length fibers, efforts have been concentrated on analyzing these failures. In addition, because of the lower stresses at which they failed, the fracture surfaces of these fibers are most amenable to fractographic analysis. For ease of reporting, the fractography on the Hughes and ITT fibers will be reported separately.

*More information concerning these fibers can be obtained in a Naval Ocean System Center Technical Report: "High Strength Fiber Waveguides."

THEORETICAL BACKGROUND

Four definitive regions surrounding fracture initiating flaws^{1,2,3} in silicate and non-silicate glasses have been observed (Fig. 1). The mirror (a flat smooth region) is bounded by the onset of mist (a region of small radial ridges) which is bounded in turn by hackle (a region of larger radial ridges) which is bounded by macroscopic crack branching. It has been extensively demonstrated that the products of the strength, σ , and the square root of the distance from the origin to the onset of: mist (i.e., the mirror radius, R_m), the onset of hackle (R_H) and of crack branching (R_B) give three constant values for silicate glasses:

$$\sigma R_i^{1/2} = A_i$$

where i refers to the mirror-mist, mist-hackle or crack branching boundaries. It has been shown that these radii are related to the initial flaw depth, a , or half width, b , through the combination of fracture mechanics and fracture surface analysis:

$$\frac{c}{R_i} = K_{IC}^2 Y^2 / 2A_i^2$$

where $c = \sqrt{ab}$, Y is a constant dependent on location and geometry of the crack and K_{IC} is the critical stress intensity factor. The mirror constants A_i and K_{IC} for silica have been previously determined. It has been shown that the fracture mirror relationship observed in bulk glasses is applicable to optical fibers.⁴ More detail of the relationships of the initial flaw sizes to the mirror radius and to fracture analysis is described elsewhere.^{3,5,6}

EXPERIMENTAL PROCEDURE

ITT fibers consist of a silica core with silicone coating and an exterior plastic coating(Hytrel). In order to examine the fracture surface of these fibers, it is sometimes necessary to strip the fiber of the outer Hytrel plastic coating. This is done manually by inserting a razor blade carefully around the fiber and then manually pulling off the severed plastic. The Hughes fibers contain a metallic coating.* When it is necessary to remove this coating the fibers are placed in an aqua regia solution for 1-2 minutes and then rinsed in water. Before examination in a scanning electron microscope, both types of fibers are coated with gold.

Three types of tested fibers were sent to NRL. These include delayed failure specimens in which fibers were wrapped around a mandrel and times to failure in air, or salt water were measured. This involves merely wrapping fiber around a mandrel of a certain radius. The radius then is related to the stress induced in the fiber. In this case a fully uniform tensile stress is not achieved, but rather a bending stress is achieved. The outer portion of the fiber is in tension and the inner portion of the fiber is in compression. The other types of tested fibers were those that were subjected to tensile stresses, i.e. either proof tested at a particular load or broken in tension on a test machine. Normally, proof testing is done by passing the fiber from one drum to another at a particular rate of speed with a drag on one drum and the load from the drag recorded. One would expect the fracture surface observations from bending or tension tests to be similar.

* In most cases aluminum.

Primarily because of the silicone coating holding the fractured glass pieces together, fracture origins could be found on 50% of the ITT fibers as contrasted to less than 10% on the Hughes fibers. The latter low yield is primarily due to the fact that there is no constraint to the shattered glass, plus the fact that the metal coating often covers the origin. Etching of the aluminum or tin with an aqua regia solution removes the metal, but in most cases the fracture origin is then lost as the metal coating was essentially holding the pieces together.

Observation of fracture surfaces on brittle materials and in particular on fibers can be misleading unless one can determine that the origin is real and is primary, that is, the main cause of failure. For example, if one observes the top view in Fig. 2 it could be concluded erroneously that a relatively large somewhat irregular mirror exists surrounding the origin. However, if care is taken to get another angle of observation (side view) one sees that in reality a chip out of the fracture surface is being observed. A true fracture mirror in most cases would not deviate from the total plane of fracture as much as indicated in the figure.

A second pitfall is that there can be more than one fracture mirror along a fiber length. In general, there is one for each break. The "primary" break (i.e. the first fracture causing failure) is identified for us by the research laboratory sending the broken fiber. One would expect the primary break to produce the largest mirror and hence the smallest stress. This would be reasonable because the largest flaw (weakest link) would cause failure corresponding to the lowest stress. However, in the limited cases we were able to examine, the secondary breaks had larger mirror radii than the

primary break. The reason for this is not known at this time. The smallest mirror reflects the true stress at failure. Thus, if one is not sure whether the break is the primary break, one can only say that the stress calculated from the fracture mirror measurements is the least that could have occurred. In the case of low strength fibers, however, there are usually only one or two fiber breaks and thus it is fairly obvious which is the primary break.

RESULTS AND DISCUSSION

Initially 25 Hughes and 20 ITT fibers were sent to NRL. All of these fibers have been examined, and the bulk of this report will describe these results. More recently we have received several "weak" fibers both from ITT and Hughes in order to aid in their production of fibers by analyzing and/or confirming the cause of the low strengths. These results will be discussed even though the analysis on some is not complete.

Hughes Fibers

Table I summarizes the 25 Hughes fibers examined to date. Note that even when origins could not be determined, fracture markings pointed back to the area of the origin, indicating whether a surface or internal origin was the source of failure. An example of this is shown in Fig. 3 where the origin is covered by aluminum but the markings clearly indicate that a surface origin was the cause of failure even though the exact origin, i.e. whether it is a crack or a dust particle, etc., is not clear. Unfortunately, many of the failure origins are lost upon fracture due to the large amount of elastic energy stored in the high-strength fibers. Nevertheless, there are some important observations and analyses that can be made. All

origins observed to date on Hughes fibers were from surface defects. These include a surface crack(Fig. 4) and a bubble which originated in the preform(Fig. 5). In the latter, the bubbles along the surface indicate that a large bubble in the preform was drawn out during fiber pulling. Even with the large defect (38 μm half-width) it's spherical shape resulted in approximately 160,000 psi(from mirror measurements) breaking stress in reasonable agreement with the approximately 200,000 psi measured during the test. Other origins were not found, but the fracture markings leading back to the surface on a few others could readily be observed as in Fig. 3. In fact, the fiber in Fig. 3A was etched in an aqua regia solution to remove the aluminum coating because it obscured the detail of the origin. Even then, the aluminum appeared coherently connected to the glass indicating that an aluminum oxide interface may be present between glass and metal. Delayed failure specimens 1 through 5 in Table I also showed a high degree of corrosion(Figs. 4 & 6), but the corrosion product has not yet been identified. As can be seen in Fig. 6 there are many cracks in the aluminum coating. Many of these cracks look like they follow the grain boundaries in the aluminum. This indicates that they could be occurring during stressing, although it is not clear that corrosion alone would not cause this. Also, it is possible that they are a result of stress corrosion cracking. One way of determining the cause of these cracks is to examine the fiber after coating and during stressing. In addition to the cracks there is evidence of roughly circular pits. One would suspect that the pits would be elongated if they occurred before or during stressing, and more circular or spherical if they occurred after stressing. Thus, one would surmise that these

pits were not preexisting.

Several low strength fibers were sent from Hughes for identification of fracture origins. Although the analysis is not complete, it is quite evident that a semi-elliptical ridge on the surface of most of the fibers examined is consistently the cause of failure (Fig. 7). Because the ridge along the fiber surface is relatively smooth it would appear that this defect is being caused in the drawing process when the fiber is relatively hot. One would expect a rough gouge if some object were pulled across the surface. Further communication between NRL and Hughes will hopefully trace the exact cause of this defect and thereby eliminate it.

ITT Fibers

Table II summarizes the results of 29 ITT fibers examined to date. Of the eighteen identified failure origins, 11 were identified as surface origins and 7 as internal sources of failure.

The surface failures were a result of a foreign particle (Fig. 8), five from cracks or mechanically induced chips (e.g. Fig. 9 and 10), and 5 "unidentified" sources of failure (e.g. Figs. 11 and 12). It is suspected that at least four of the last 5 listed are from small crystallite formations, but this has to be determined for certain.

A foreign particle is shown attached to the silica in Figures 8 and 13. The particle was analyzed using an electron microprobe; the results indicated the presence of magnesium and iron as well as silica (Fig. 13). This type of failure can be avoided by filtering (clean room). This "dust" particle which attached to the fiber during drawing caused a small (approximately 1.5 μm) crack, most likely upon cooling, which subsequently lead to failure. The size of this crack (2 μm) is in

good agreement with the calculated $3 \mu\text{m}$ from Eq. 2.

Although most fractures were from surface origins, there are seven cases where internal origins occurred. One internal origin was an inclusion containing rare earth elements (Nb and La) Fig. 14. This failure occurred due to a ($0.2 \mu\text{m}$) crack formed between the inclusion and bulk SiO_2 . Failure from inclusions related to natural forming elements can most likely be eliminated by using synthetic quartz material rather than the natural quartz. This also applies to preform manufacture used in the CVD process. If the outer tube or preform material is natural quartz, then defects such as bubbles and inclusions will be transferred to the final silica fiber. Closer examination is planned to determine the source of these internal failures. Higher magnification is required to determine the source of these failures because the size of the defect, in most cases, is less than $0.2 \mu\text{m}$, and consequently detailed analysis is difficult.

Several fibers were sent that were known to have low strength values. Fracture surface analysis determined that the low strength (approximately 200,000 psi) failures were probably occurring due to a defect that existed in the preform and was drawn out during the pulling of the fiber. This is concluded because there were several internal failures in the same general location in the plane of the fracture (cf Fig. 15a and b).

In addition, a step index fiber was examined and was found to most likely fail from the interface between the inner and outer core. This step index fiber is now being studied in more detail.

The fracture stress of all fibers except three in Table II agreed with those expected from mirror measurement (i.e. Eq. 2). The first

two (ITT-3, ITT-4) have lower stresses than measured from the proof stress because these failed before the full stress was achieved on the drum. The difference for the third (770510-1) is unknown.

ITT-NOSC Fibers

Of all the fibers observed (28 pairs) which were sent from NOSC, only two origins were found. The low yield is due to the fact that these fibers all had a relatively high strength since the pretest proofing at 300 ksi eliminated the weak fibers. These high strengths > 500 ksi mean that fracture origin determination is very difficult, if not impossible. However, two of the three fracture surfaces were similar in appearance (Fig. 15) to each other but not to any other fibers observed, either from ITT or Hughes. The large semi-elliptical sections in the interior of the fibers observed in Fig. 16 should have caused low strength breaks. The reported strength is $\sim 3500 \text{ MN/m}^{3/2}$ ($\sim 500 \text{ ksi}$), indicating that these fractures are probably secondary, rather than primary breaks. However, the question arises of why these large inhomogeneities did not cause failure at lower stresses as the primary break. Perhaps, because these inhomogeneities are SiO_x of a slightly different composition than SiO_2 , they were not high stress concentrators leading to low strength failure. The composition and identity of these anomalies is unknown but further research is being performed.

CONCLUSIONS

1. The usefulness of fracture surface analysis is to identify the low strength (or unusual) failures in order to correct processing or handling procedures to improve the fiber and get a higher

yield of "good" fiber.

2. High quality glass should be used in all phases of the fiber process because the weakest link theory is applicable to fiber processing, e.g. a defect or bubble in the tube used in the CVD process could be transported to the final fiber.
3. Most of the low strength failures of optical fibers are caused by defects in the preform (such as bubbles) being drawn through in the fiber process, foreign particles or "stones" from naturally occurring elements, mechanical damage during drawing, or contamination during drawing. One or several of these causes could occur in any run.
4. Only a small number of fracture origins were identified on Hughes fibers because of the coatings which tend to obscure the origin. More origins will probably be found in the future because lower strength breaks will be sent. Other means of stripping the metal coating will also be studied and could yield a higher number of observed origins.
5. Many fracture origins have been found on ITT fibers, but not enough fibers of different varieties (tensile tests vs mandrel vs delayed failure) and low strengths have been sent for statistical meaning to be given to the failure sources.
6. The stress levels for ITT-NOSC fibers have been too high (proof tested at ~ 300,000 psi) to expect a large number of observable origins. However, this problem has been discussed and primarily low strength breaks will be sent in the future.

FUTURE PLANS

1. Continue to analyze low strength (< 200 ksi) failures to try and eliminate their source.
2. Attempts to identify whether the observed break in a Weibull plot of glass fiber failures can be correlated with a change in the type of fracture origin.
3. Examine a variety of failures so that, for example, the results of mandrel and tensile tests can be compared.
4. Comparison of delayed failure fracture surface analysis with fracture mechanics predictions of times to failure, i.e. comparison of flaw size measurement and prediction.
5. Further study of secondary breaks so that primary and secondary fractures can be distinguished. This will be especially useful in the future for determining the source of any unexpected in-service failures.

References

1. E.B. Shand, "Breaking Stresses of Glass Determined from Dimensions of Fracture Mirrors," J. Amer. Ceram. Soc., 42, [10], 474-77 (1959).
2. J.W. Johnson and D.G. Holloway, "Shape and Size of Fracture Zones on Glass Fracture Surfaces," Phil. Mag., 14, [130], 731-43, (1966).
3. J.J. Mecholsky, R.W. Rice and S.W. Freiman, "Prediction of Fracture Energy and Flaw Size in Glasses from Measurements of Mirror Size," J. Amer. Ceram. Soc., 57, [10], 440-43, (1974).
4. R.D. Maurer, R.A. Miller, D.D. Smith and J.C. Trondsen, "Optimization of Optical Wave Guides-Strength Studies," Corning Glass Works TR, ONR Contract #N00014-73-C-0293 March 1974.
5. J.J. Mecholsky, S.W. Freiman and S.M. Morey, "Fractographic Analysis of Optical Fibers," Bull. Amer. Ceram. Soc., accepted for publication.
6. D.A. Krohn and D.P.H. Hasselman, "Relation of Flaw Size to Mirror in the Fracture of Glass," J. Amer. Ceram. Soc., 54, [8], 411 (1971).

Table I - Hughes Fibers

Designation	Fracture Stress		Measured Flaw Size μm	a/b	r, μm	r, μm	Calculated		Comments
	ksi	MN/m ²					Fracture Stress ksi	Fracture Stress MN/m ²	
H-SS-1 DF	200	1400							Corrosion product; pitting in Al
-2 DF	200	1400	.3		4	5	160	1100	Corrosion product; surface origin
-3 DF	200	1400							Corrosion product
-4 DF	200	1400							Corrosion product
-5 DF	200	1400	.75	2.0	4.25	5	157	1080	Cor prod; surf orig-def in preform
-6 M	400	2800							No orig pres; plastic def of Al
-7 M	400	2800							No orig pres; plastic def of Al
-8 M	400	2800							No orig pres; plastic def of Al
-9	600	4200							Prob high stress-Al cov surf orig
-10	600	4200							No orig pres; prob surface
-11	360	2520							No orig pres; prob surface
-12	360	2520							No origin present
-13	400	2800							No orig pres; prob surface origin
-14	450	2800							No orig pres; plastic def of Al
-15	550	3850							No orig pres; plastic def of Al
-16	500	3500							No orig pres; plastic def of Al
-17	500	3500							No orig pres; plastic def of Al
-18	650	4550							No origin present
-19	700	4900							No origin present
-20	750	5250							No origin present
-21	200	1400							No origin present
-22	200	1400							No origin present
-23	200	1400							No origin present
-24	200	1400							Origin covered by (fused to?) Al
-25	200	1400							No origin present

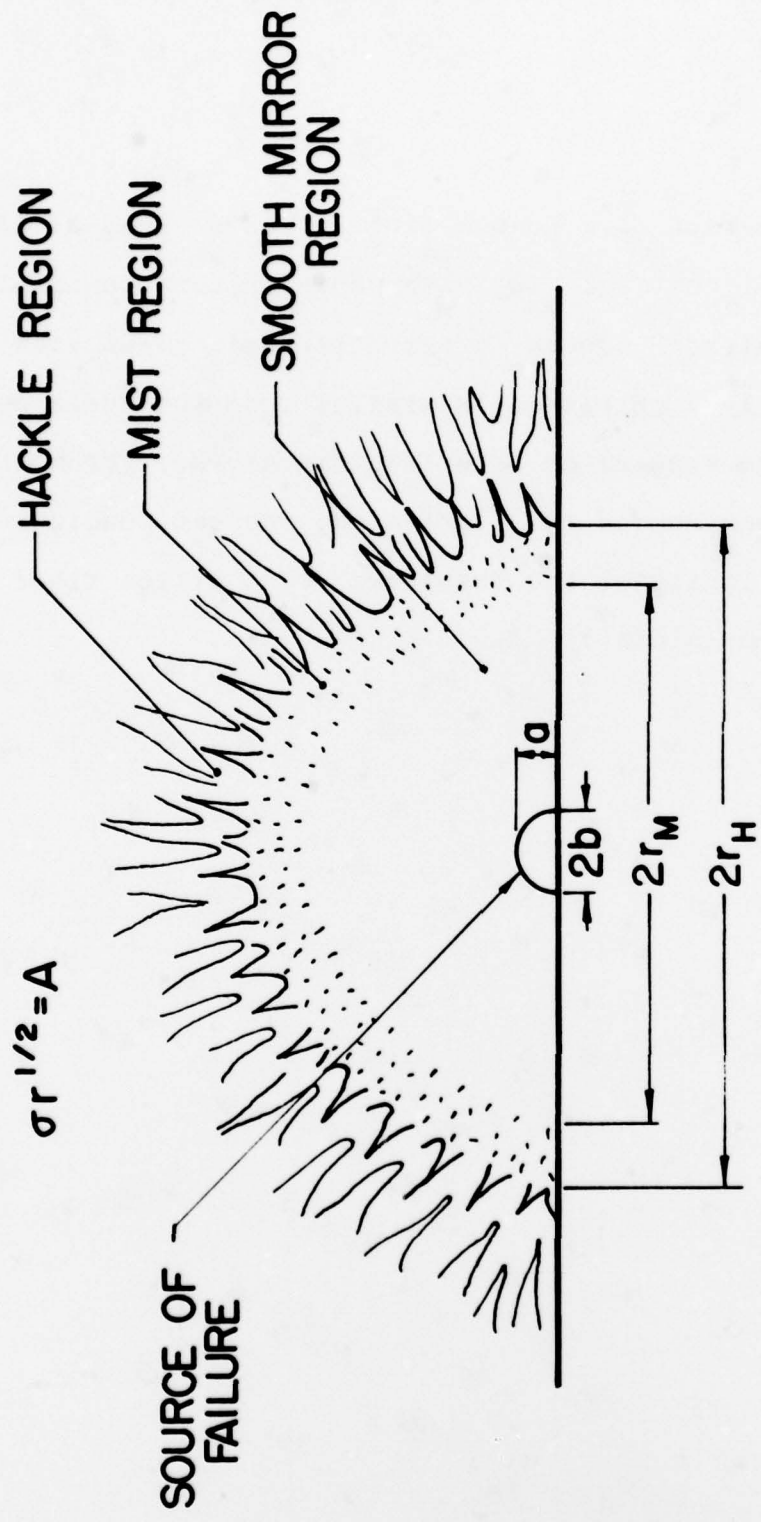
D.F. = Delayed Failure; M = Mandrel

Table II - ITT Fibers

Designation	Fracture Stress ksi	Fracture Stress MN/m ²	Critical Flaw Size Meas Cal μm	a/b	r _i	r _o	Calculated Fracture Stress ksi	Calculated Fracture Stress MN/m ²	Comments
ITT-1 T08 P	200	1400	0.2	0.8	2.5		200	1400	Prob on surf; rough structure
-2 T08 P	200	1400	0.2	0.8	2.5		200	1400	Int incl-Nb,La, crack at edge 5μm _{incl}
-3 T08 P	200	1400	2	0.5	50	59	46	315	Surface crack
-4 T08 P	200	1400	2	0.3	45	50	49	340	Fail. from dust part. Mg&Fe ~ 10 μm
-5 T08 P	200	1400	5	0.7					Rough struc. lg chip at origin lip
ITT-1SS P2/77	346	2400	.08		1	1.5	300	2070	Rough Structure/Surface
2SS P	346	2400							Origin lost; fiber non-concentric
3SS P	346	2400							Lost origin
4SS P	346	2400	.04		.5	.75	400	2794	Rough surface
ITT-770510-1	72	500	.15		2	2.5	225	1550	Surface failure, chip?
-2	117	800	.9		12	14	94	645	Surface crack?
-3	69	475							Origin missing/surface
-4	210	1450							Origin missing
-5	859	5900							Origin missing
-6	196	1350							Origin missing
-7	470	3250							Origin missing
-8P	300	2100							Origin missing
-9P	200	1400	.2		2.5	3	200	1400	Internal origin
-10	435	3000	.09						Surf origin/rough surface; DF:H ₂ O
-11	435	3000							Origin missing DF; H ₂ O
770729-1P	100	700	1		7.5	9	116	800	CVD-surf crack edge of irreg defect
-2P	100	700	.2		6	7	130	900	CVD-int. orig hole or inclusion
-3P	300	700							CVD-origin missing
ITT-770708-1P	100	700	0.5		6.5	8.5	123	850	Int. failure near edge of fiber
-2P	100	700							Origin not found
-3P	100	700	0.4		5	6	144	990	Int. failure near edge of fiber
-4P	100	700							Int. failure/origin covered
-5P	100	700	0.4		~5	~6	144	990	Int. failure near edge of fiber
-6SI			2		~40		55	382	Int. at edge of step index; hole present but not origin!

P=Proof Stressed; DF=Delayed Failure; SS=Supersil

Fig. 1. Schematic of fracture origin showing idealized semi-elliptical surface flaw and surrounding fracture features known as mirror, mist, and hackle. Crack branching is beyond the hackle.



SHAPE AND GENERAL APPEARANCE OF FRACTURE MIRROR SURFACES WITH FLAW.

Fig. 2. SEM fractograph of a Hughes fiber (770209- H-SS-3) after removal of metal coating. Top view shows appearances of irregular "fracture mirror" around "origin" (arrow). Side view shows this to be really a chip that is missing from the surface (arrow) giving the false appearance of a fracture mirror. From the fracture markings beyond this lost area, one can conclude that a surface defect initiated the fracture. (The silica fiber is nominally 120 μm in dia.).

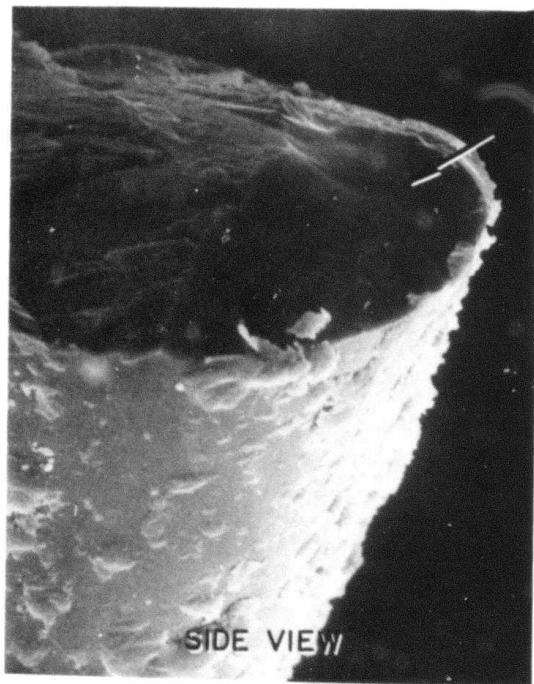
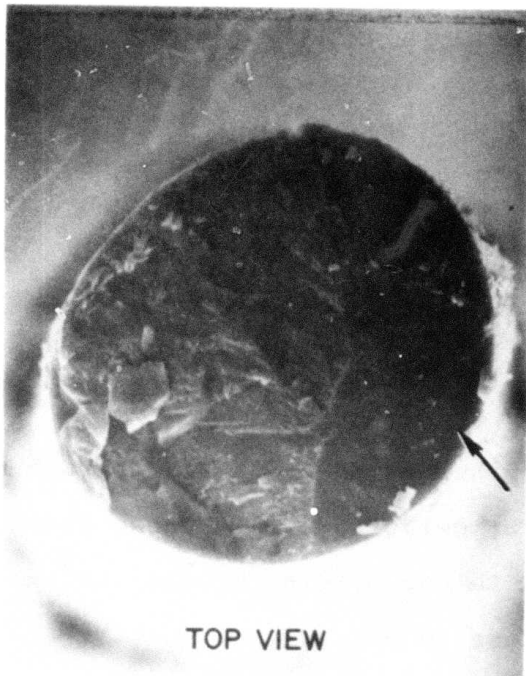


Fig. 3. Matching halves of a SEM fractograph of Hughes fibers
(A-770725-37b; B-770725-37a). These show that fracture features
"point" back to the origin (arrows) at the surface even though
the exact cause is unknown.

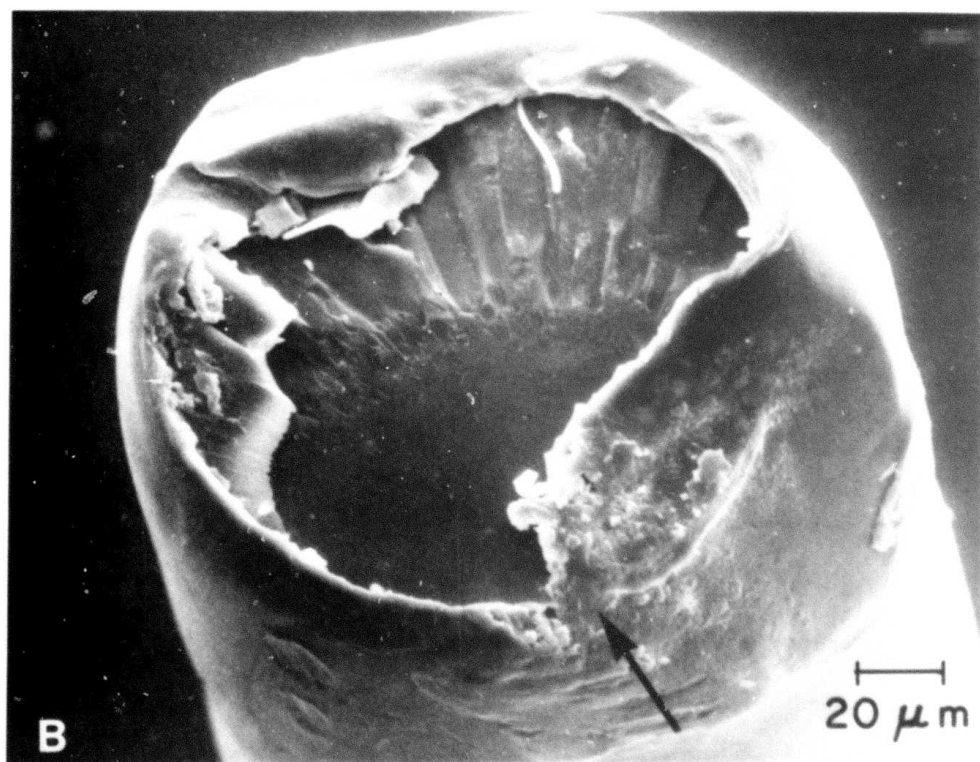
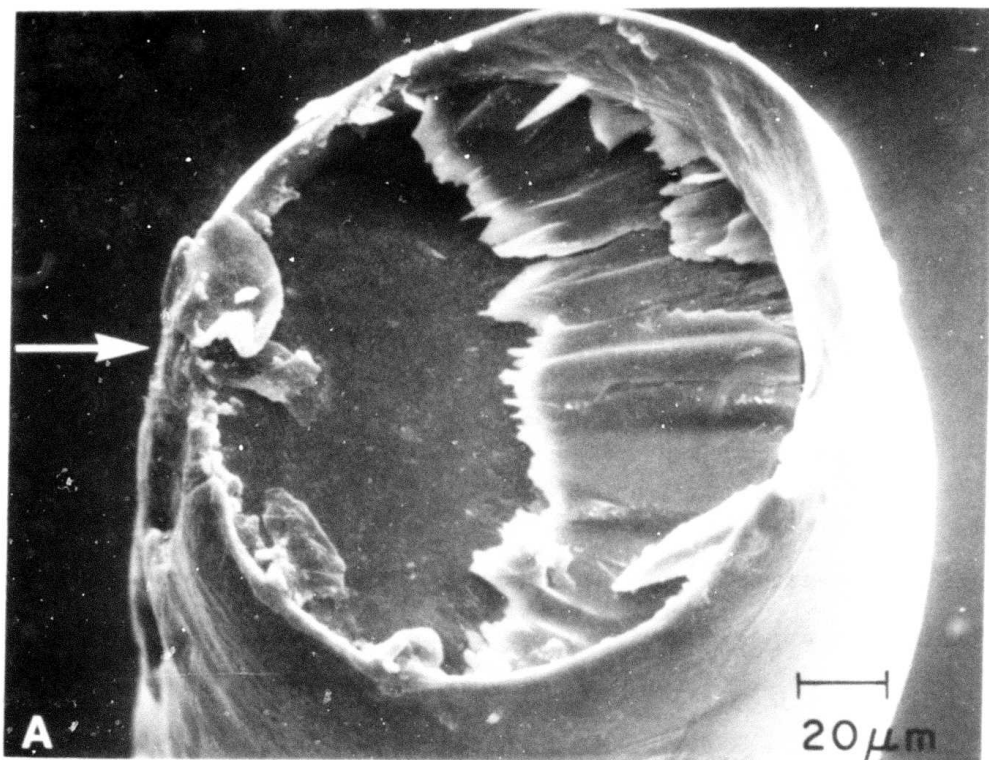


Fig. 4. SEM fractograph of a Hughes fiber (770209 - H-SS-2) showing fracture demarcations surrounding the fracture origin (most likely a sharp crack-not visible on the surface).

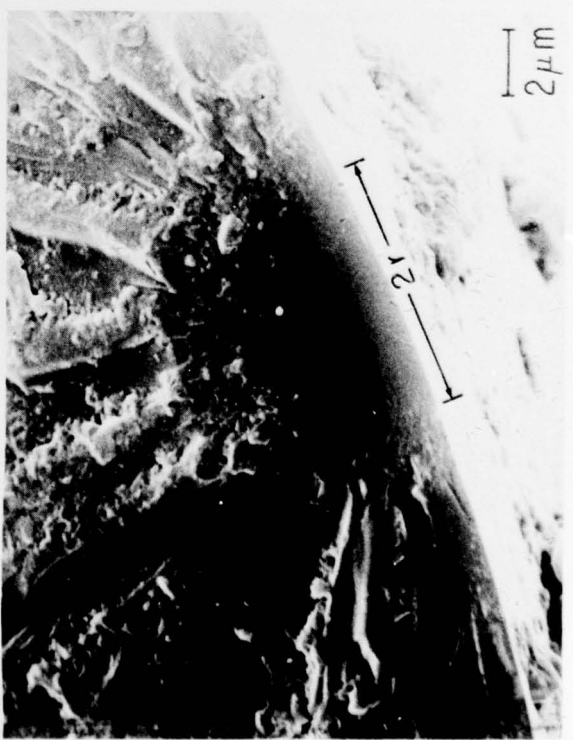
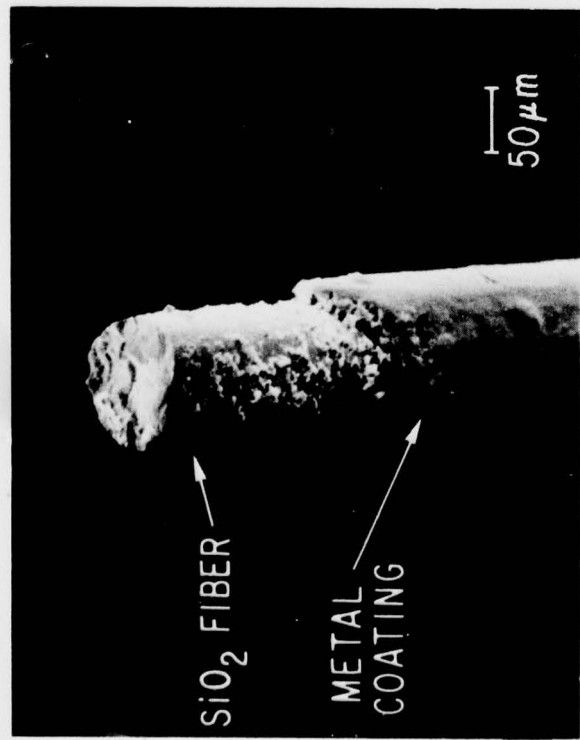
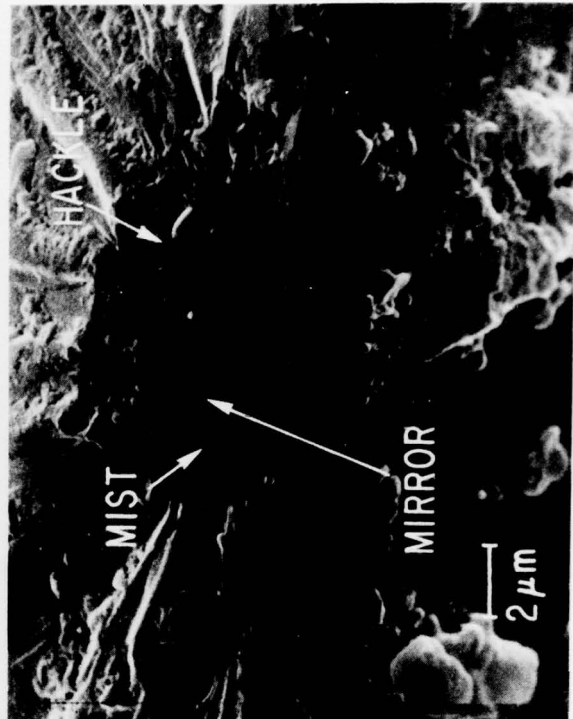
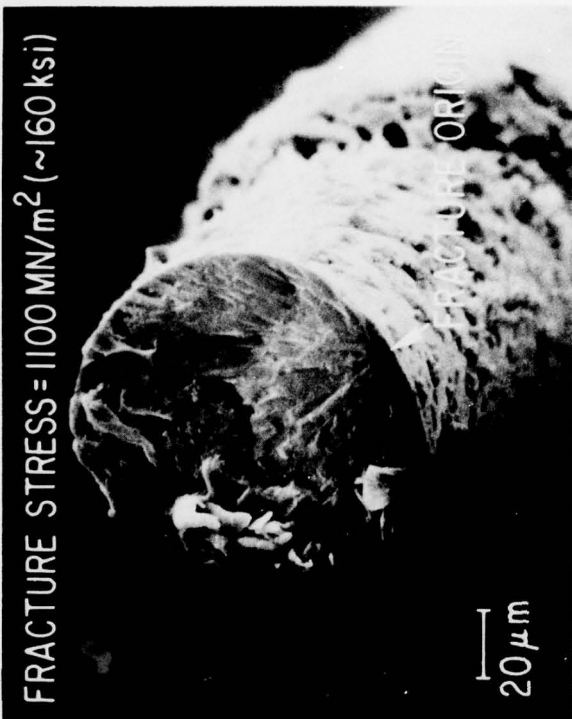


Fig. 5. SEM fractograph of a Hughes fiber (770209 - H-SS-5) after removal of the metal coating. Source of failure (arrow) is from an elliptical defect, most likely from a bubble in the preform that was drawn out with the fiber.

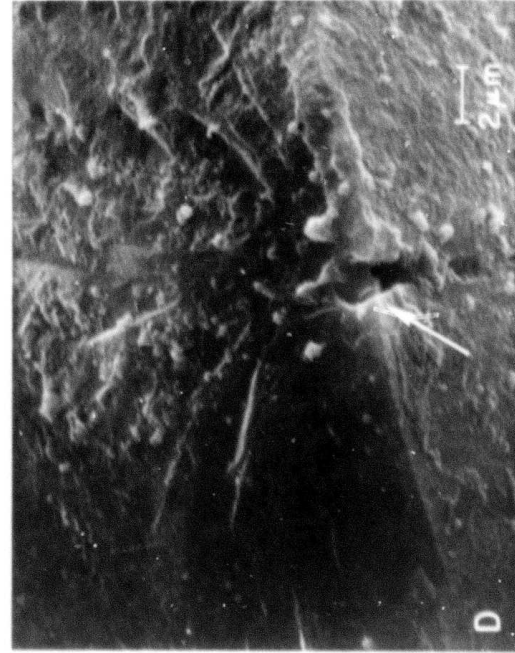
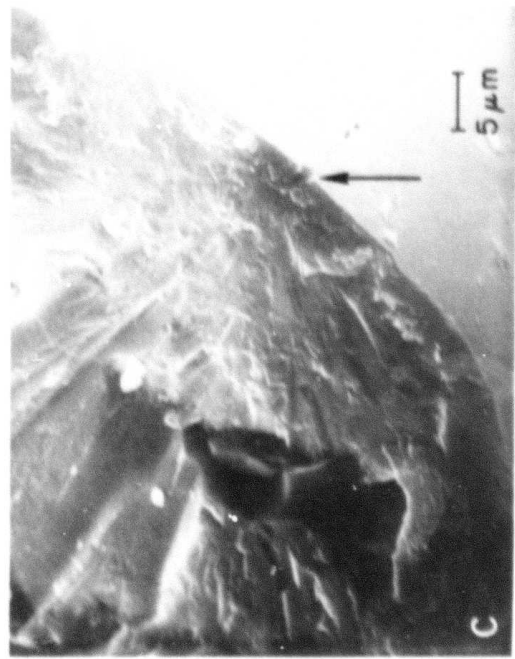
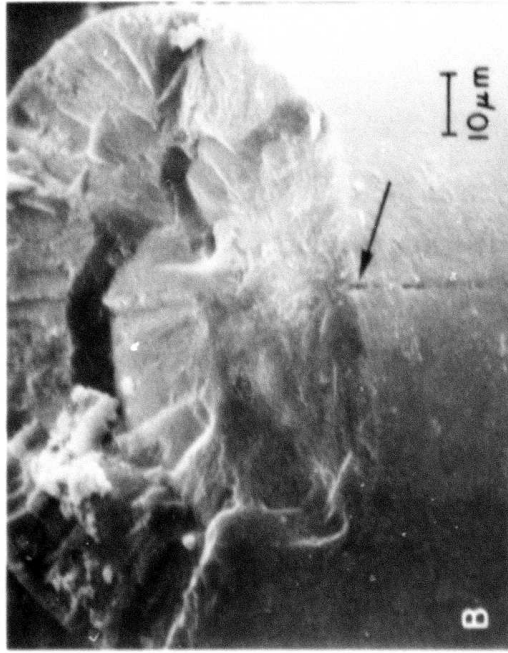


Fig. 6. SEM micrograph of the corroded surface of metal and fiber as a result of failure in salt water. (Hughes fiber 770209-H-SS-1). Notice the cracks in the metal tend to follow grain boundaries (C and D).

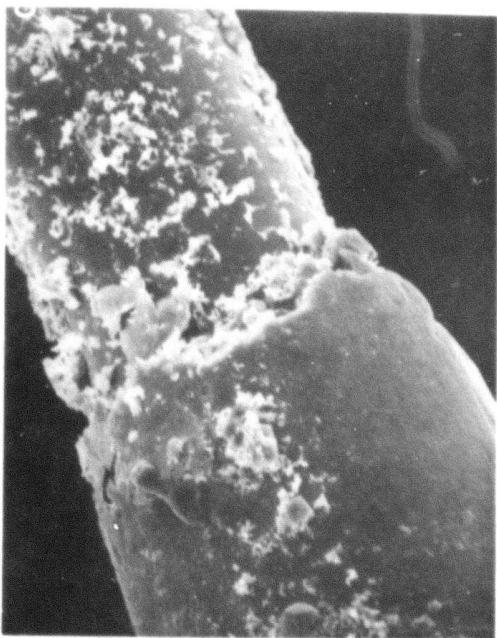
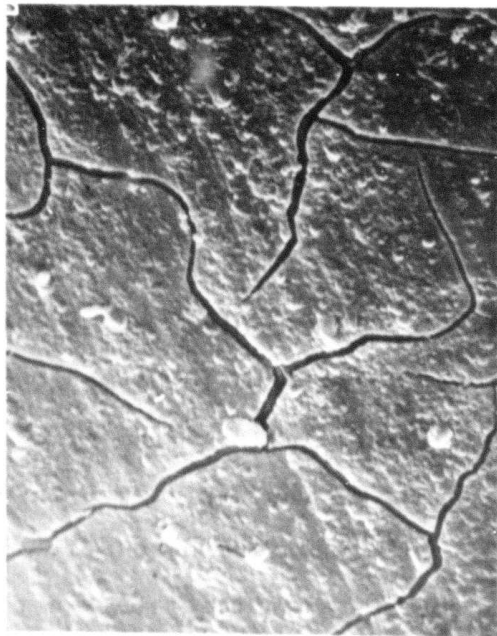
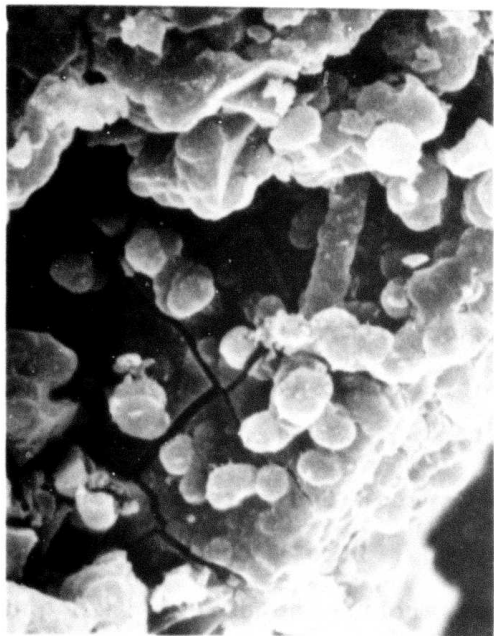


Fig. 7. SEM fractograph of four Hughes fibers failed in proof test at relatively low strengths. Notice that all fibers indicate surface failure from an elliptical cut with ridge. The smoothness of the depression in B and C would indicate this occurred while the fiber was soft. Also, most likely the metal is debonded from the fiber in the area around the defect in B and C. (770725-: A-4a; B-2a; C-1a; D-3)

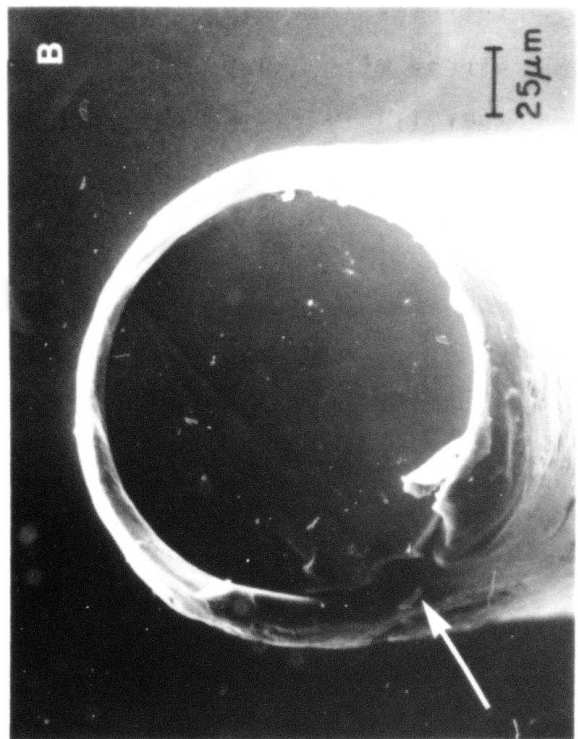
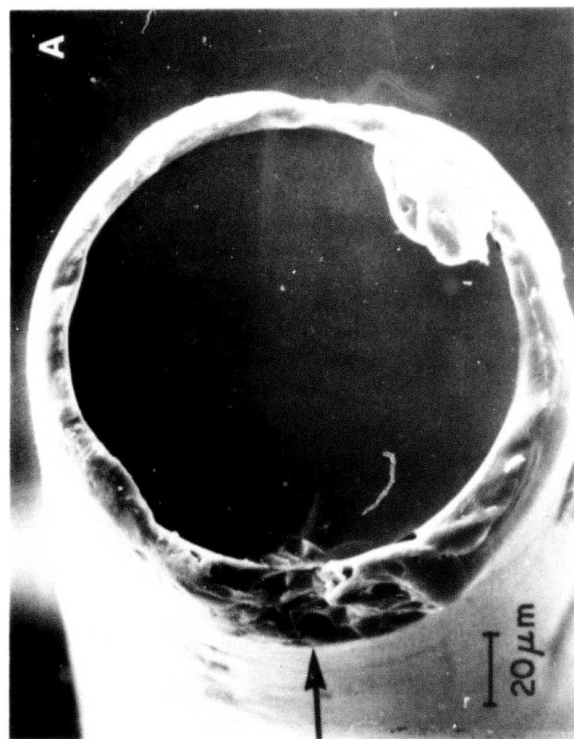
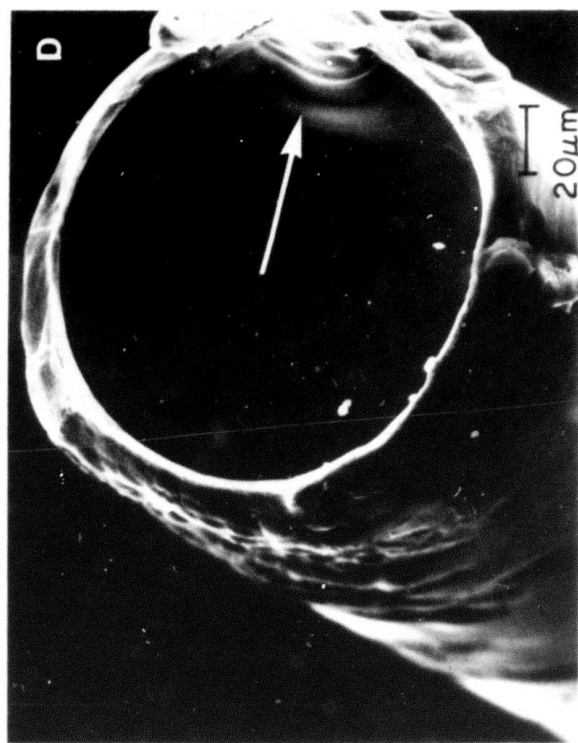
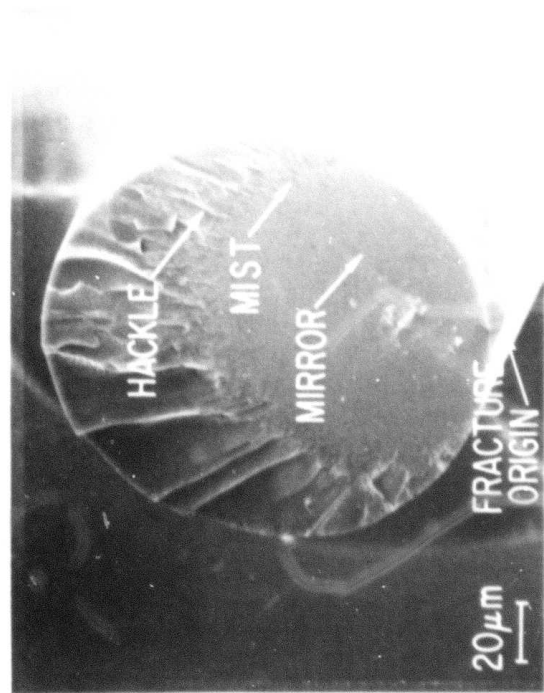
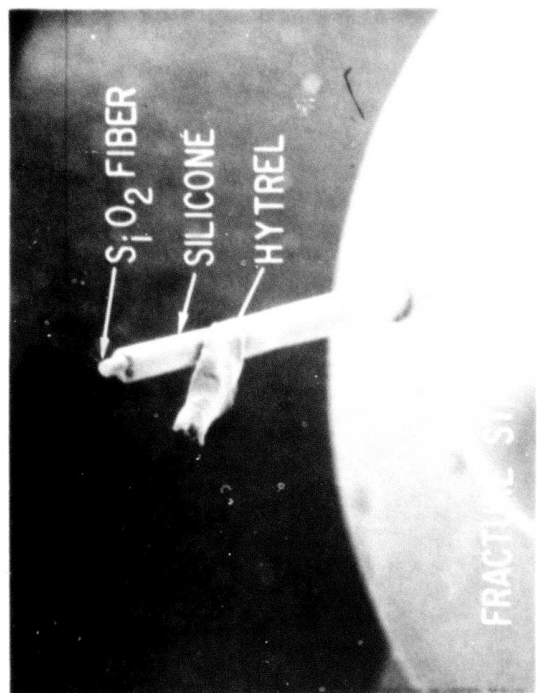
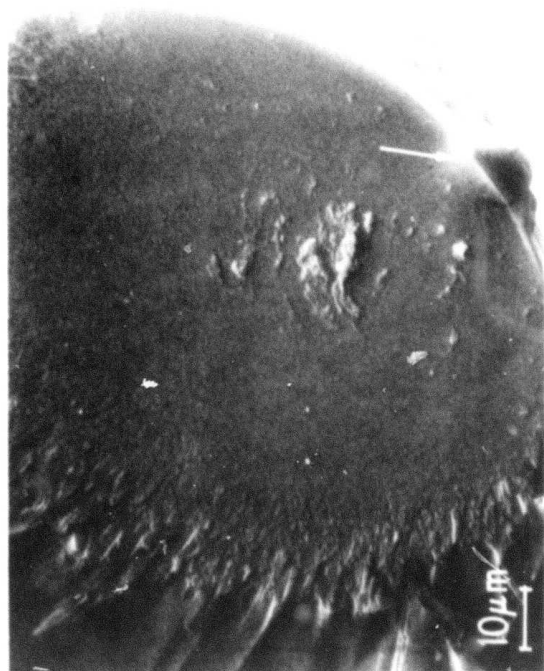
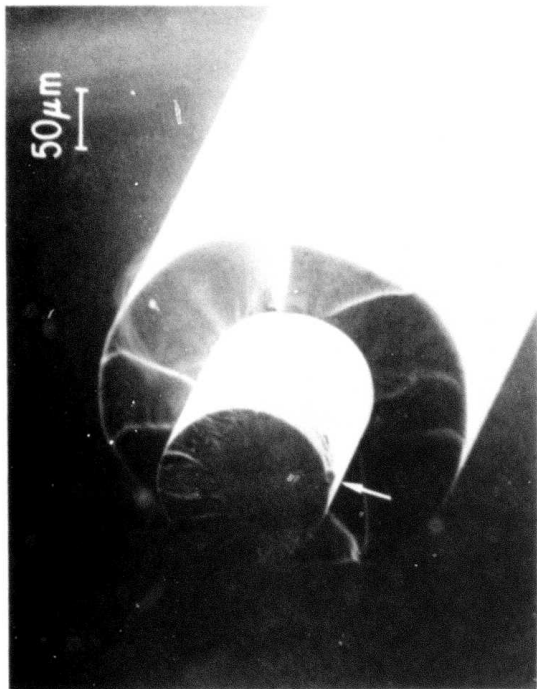


Fig. 8. SEM fractograph of an ITT fiber (761221-4) that failed in a proof test (200 ksi). The source of failure (crack between foreign particle and bulk SiO_2 , as shown in lower right) is shown surrounded by the fracture demarcations (lower left). The foreign particle is identified as containing Mg, Fe, and Si (cf Fig. 13). The 'mirror' size measurements indicate a failure stress of $\sim 315 \text{ MN/m}^2$ ($\sim 45 \text{ ksi}$). This means that this fiber most likely failed before the full proof stress was achieved, i.e. around the edge of the drum.




The image shows a scanning electron microscope (SEM) fractograph of an ITT fiber. The fiber surface is mostly smooth but exhibits a sharp, jagged crack that runs diagonally across the lower right portion of the image. A dotted line is drawn along the path of this crack. The overall appearance is that of a brittle fracture surface.

Fig. 9. SEM fractograph of an ITT fiber (761221-3) that failed from a sharp crack at the surface (dotted line in lower right). As in Fig. 8, this fiber failed well below the proof stress of 1400 MN/m^2 indicating failure on the edge of the drum before full stress was achieved.

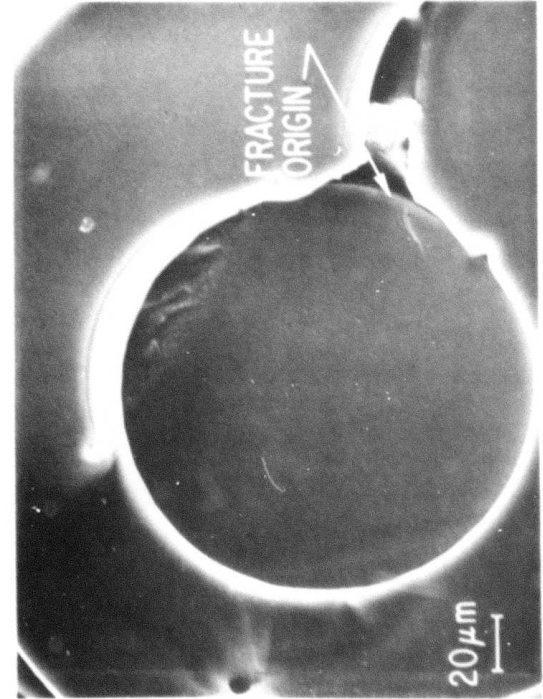
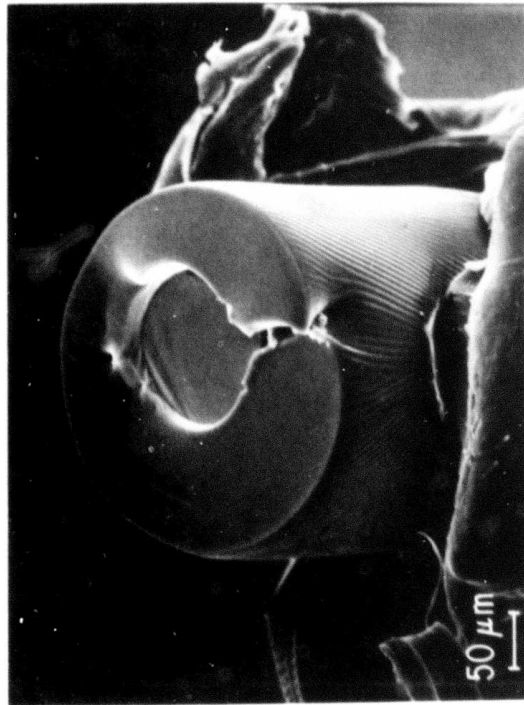
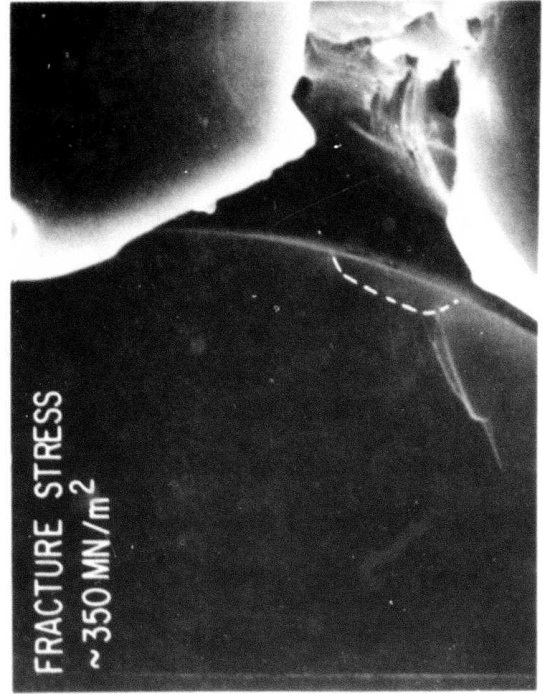
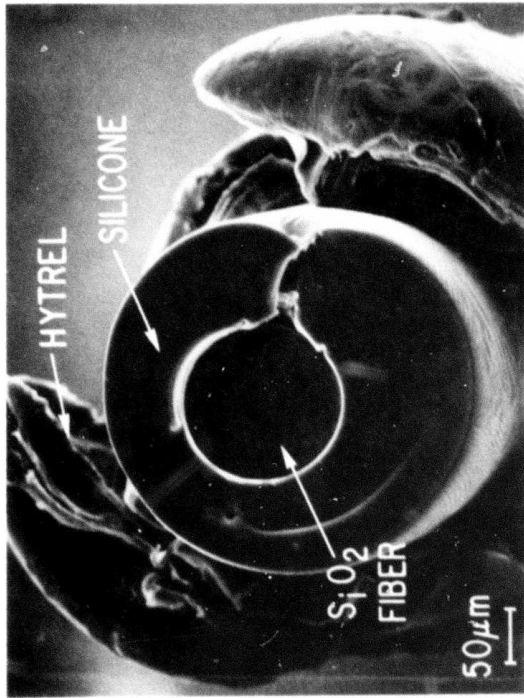


Fig. 10. SEM fractograph of an ITT fiber (761221-5) that failed from a mechanically induced crack. Although the crack is relatively large, it is probably not sharp, and thus, this fiber most likely achieved the 1400 MN/m^2 proof stress.

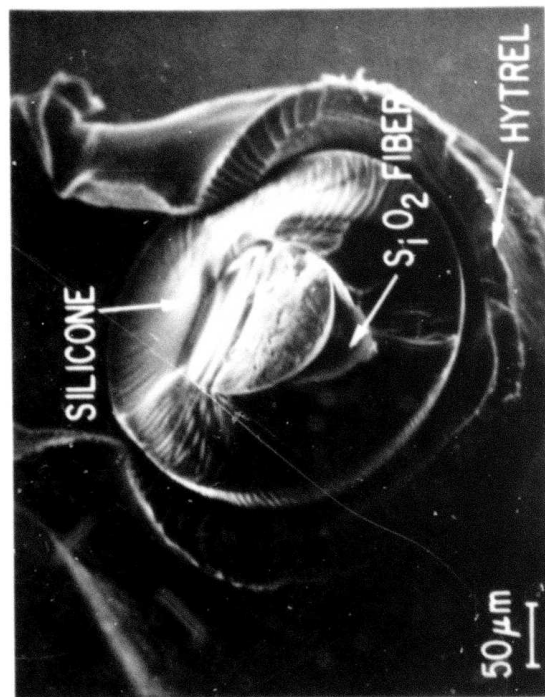
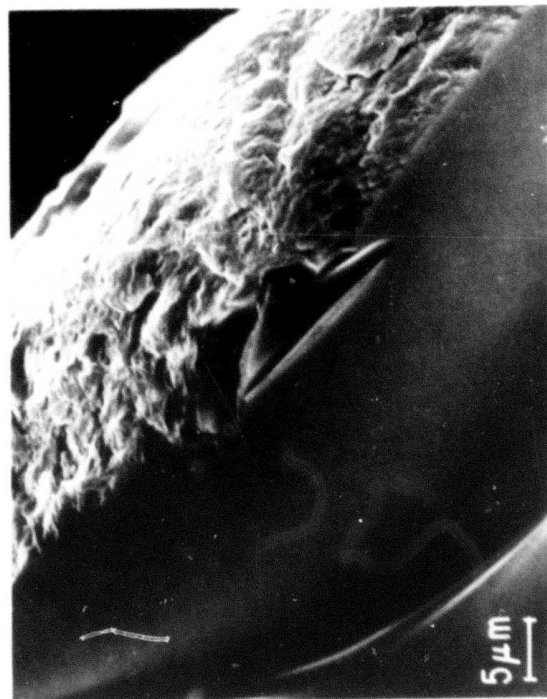
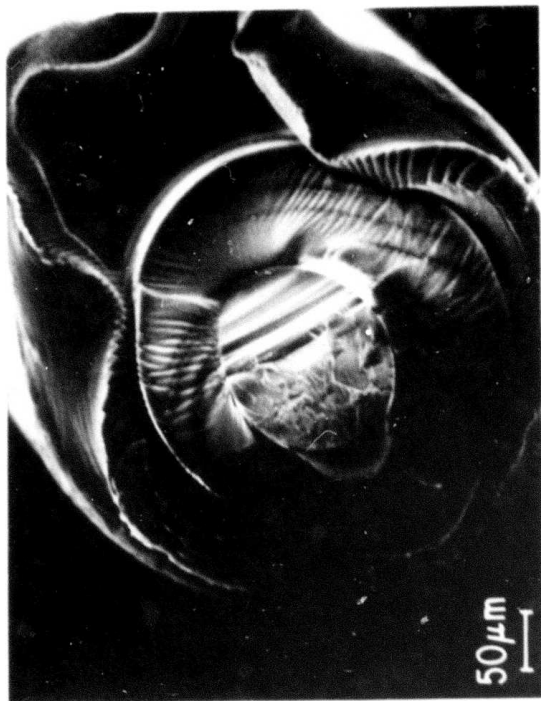


Fig. 11. SEM of an ITT fiber (770209-A) failing from the surface. The nature of the fracture origin and surrounding area (rough surface) indicates a high stress ($> 2100 \text{ MN/m}^2$). The exact source of failure is unknown.

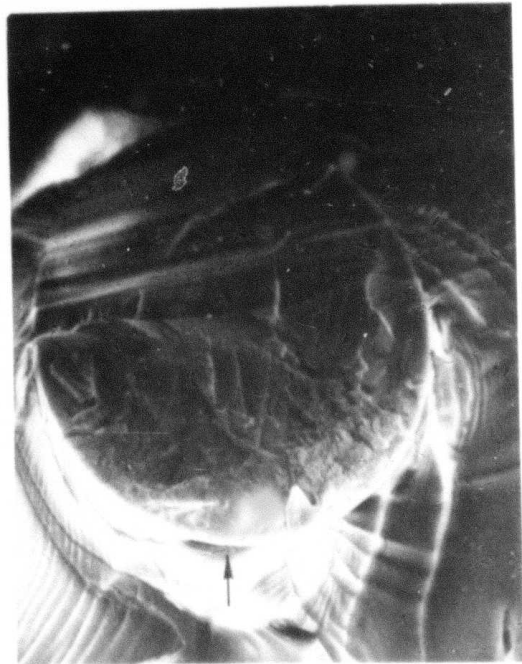
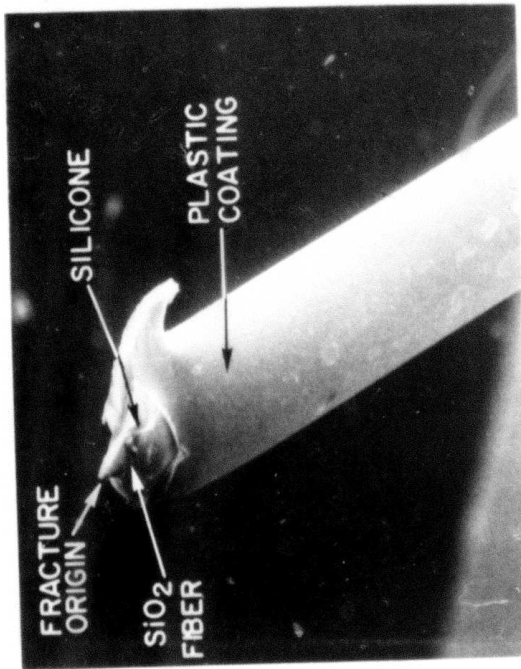
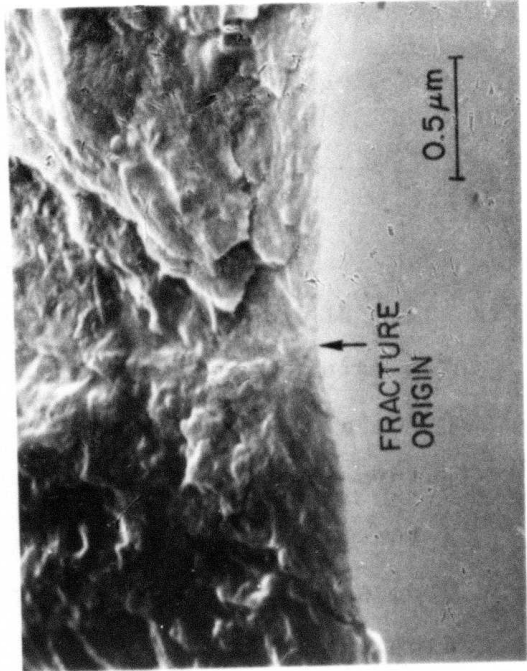
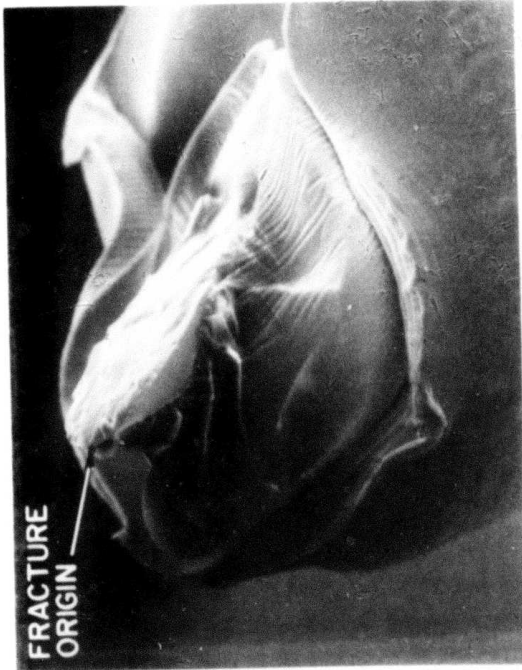


Fig. 12. SEM of an ITT fiber (770209-1) failed from the surface.

The nature of the rough area surrounding the origin (arrow in B, C, and D) indicates a high stress ($\sim 2070 \text{ MN/m}^2$). The exact nature of the fracture origin is unknown, but could be due to a thermal expansion mismatch between two phases (i.e. glassy SiO_2 and crystalline SiO_2 or crystalline metal or crystalline alumina).

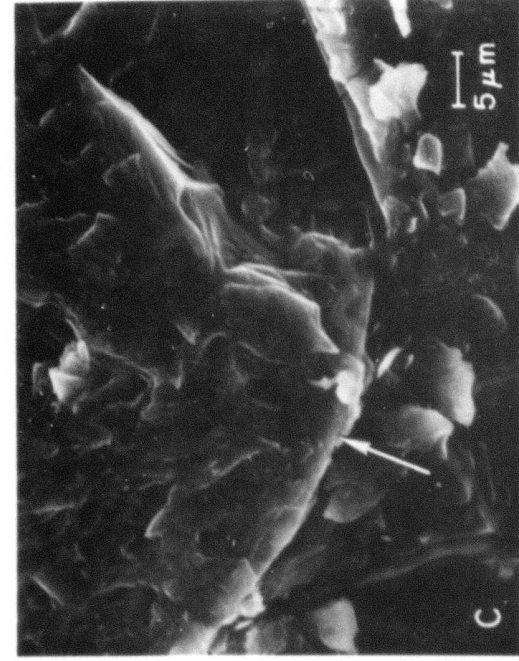
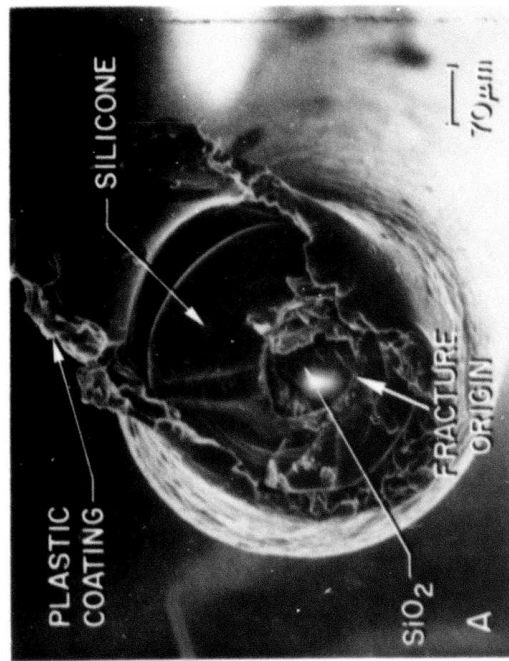
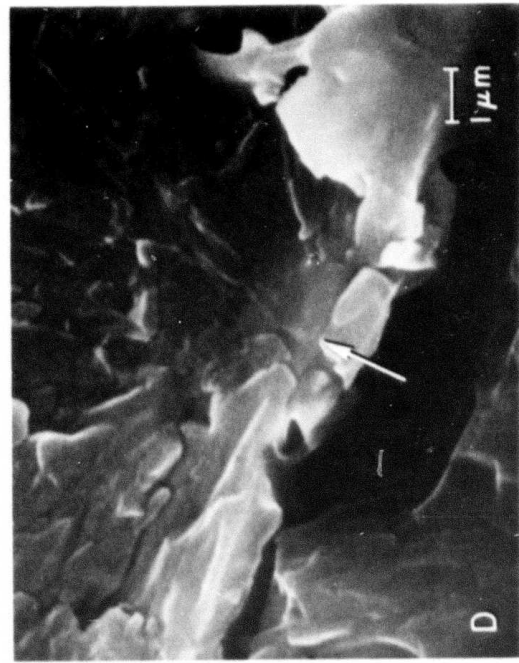
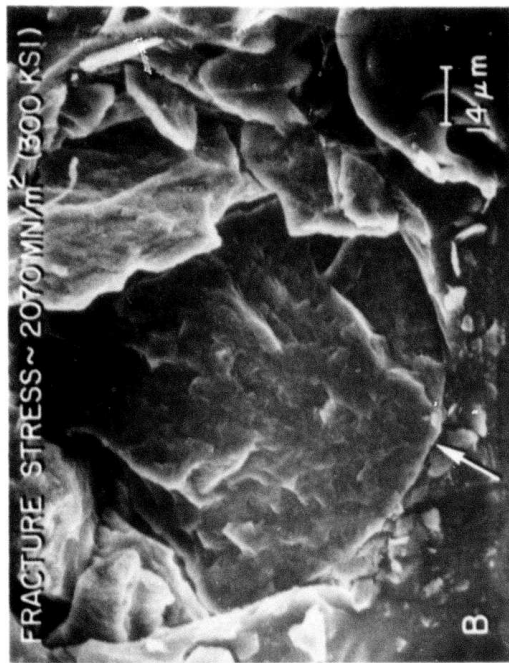


Fig. 13. A) SEM fractograph of Fig. 8 for reference. B) Real image of A as given by microprobe unit. C and D) Microprobe electron images showing relative concentrations of Fe and Mg, respectively. Arrows indicate fracture origin for reference.

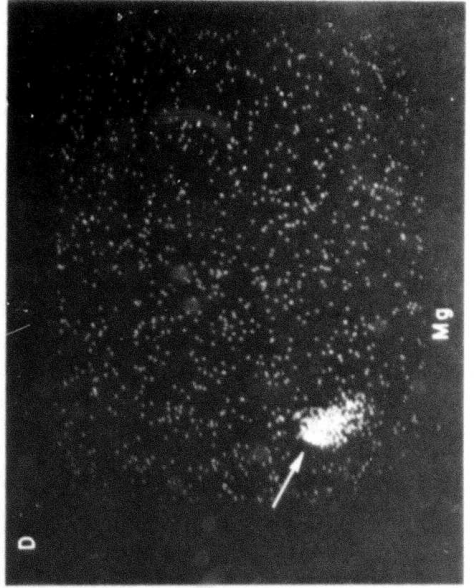
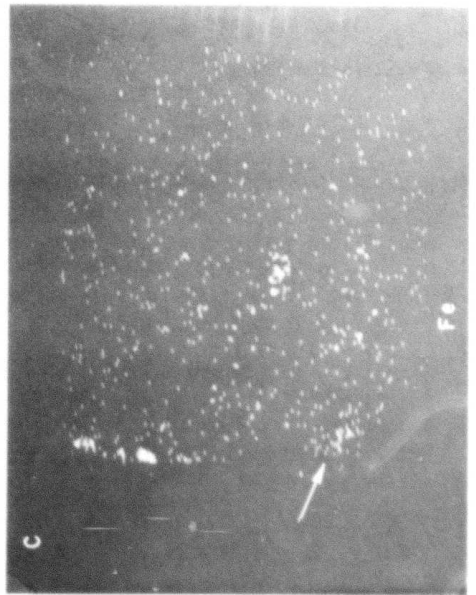
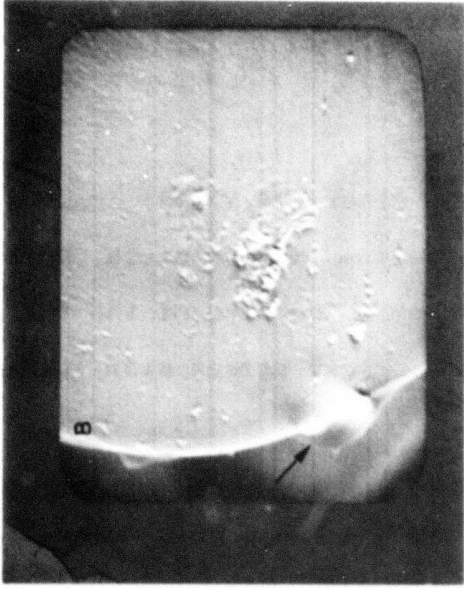
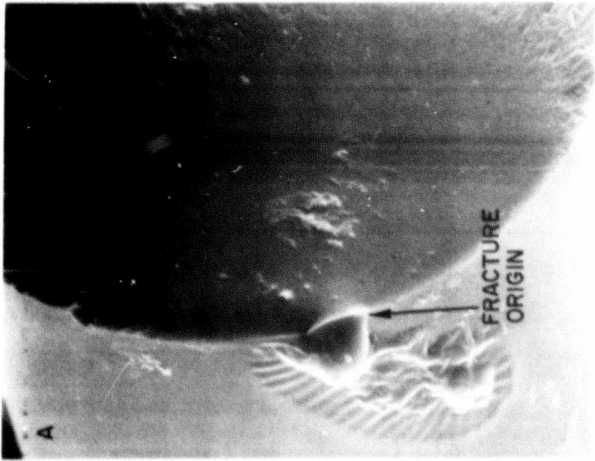


Fig. 14. SEM fractograph of an ITT fiber (761221-2) showing failure from a crack at the interface between a rare earth (Nb and La) inclusion and the bulk SiO_2 fiber. The size of the fracture "mirror" region surrounding the origin agrees with the 1400 MN/m^2 proof stress recorded.

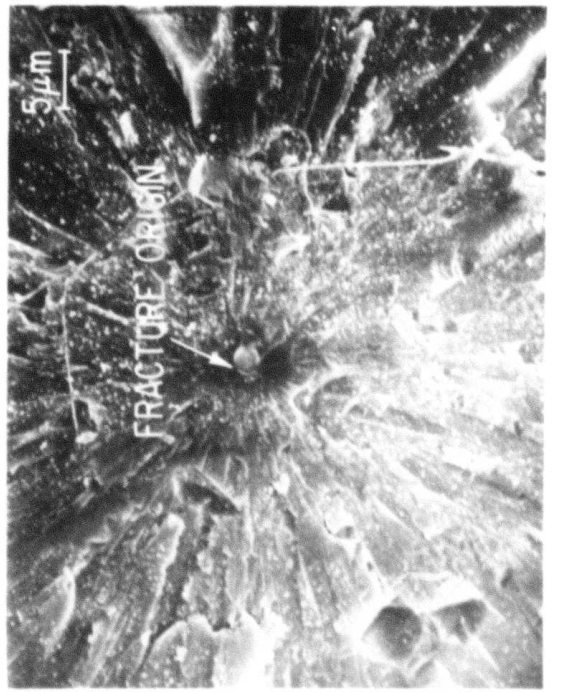
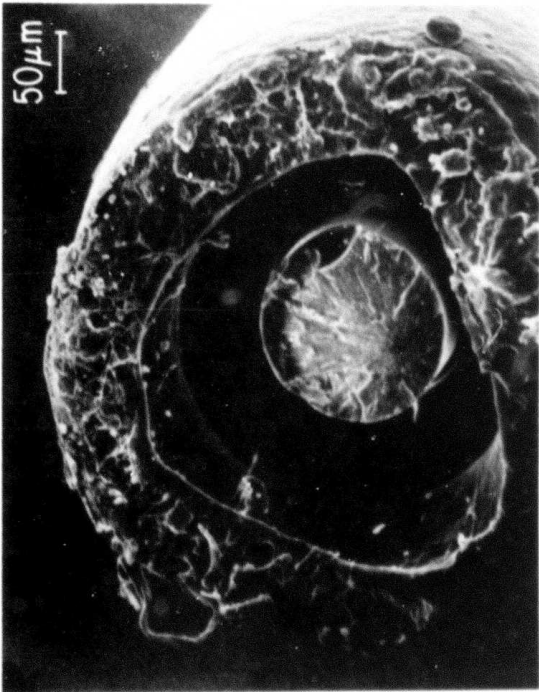
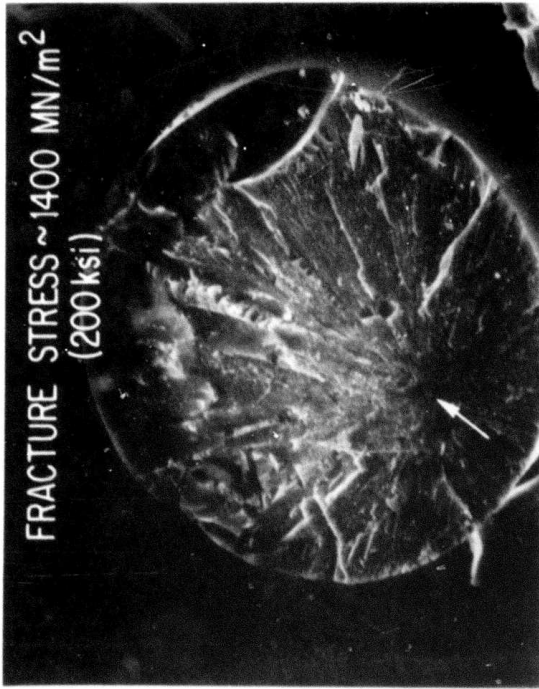


Fig. 15. SEM fractographs of three ITT fibers failing from internal sources. (A=770708-4; B=770708-3; C and D=770510-9.) The location of the origin in A & B and the other fibers of this set (Table II) indicate that the same type of source is probably causing failure. Although not certain, the white dot evident in D could be a small microcrystallite of silica.

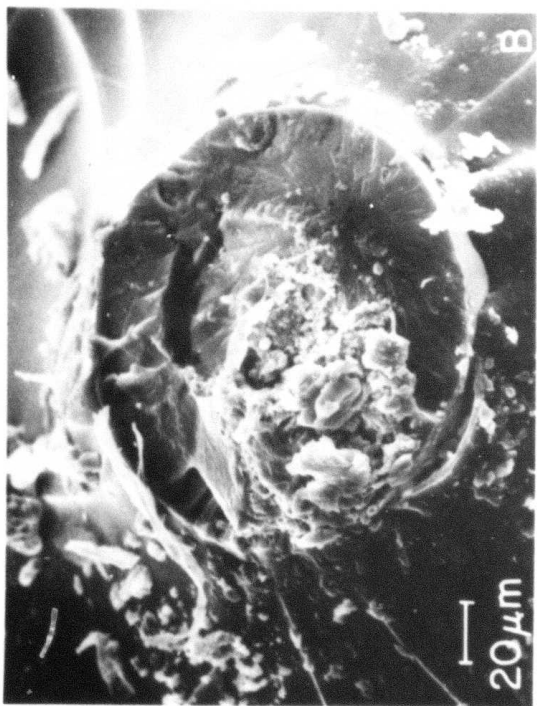
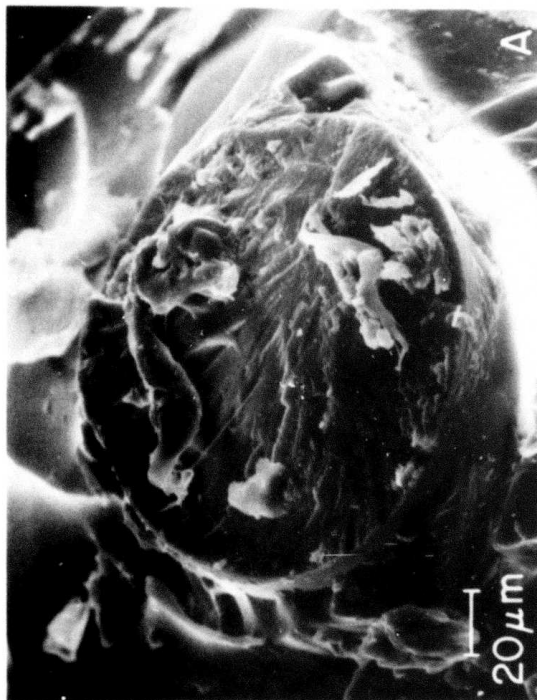
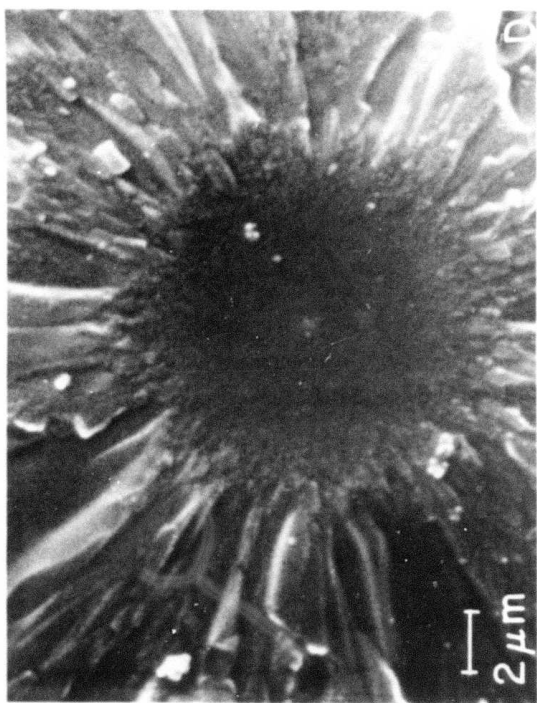
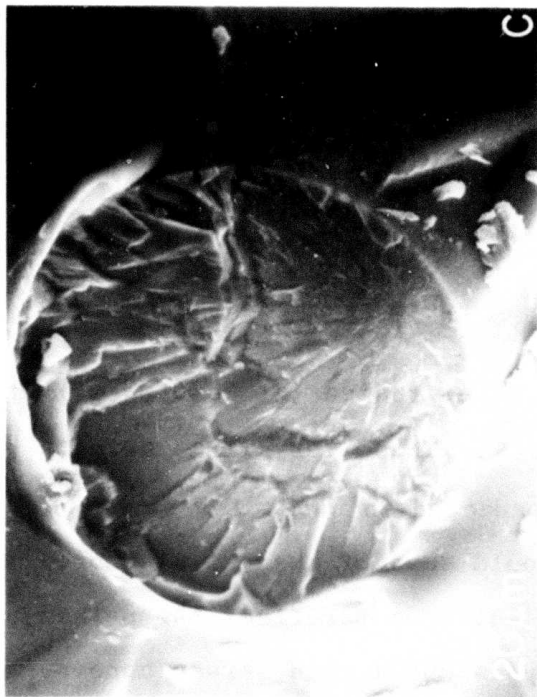
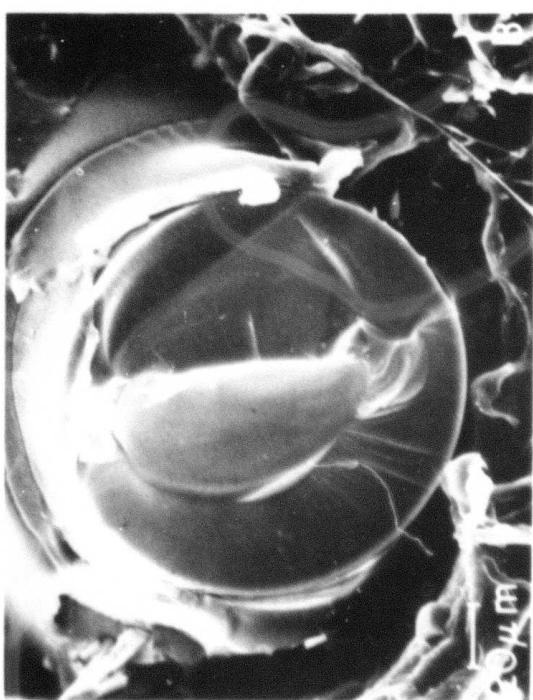
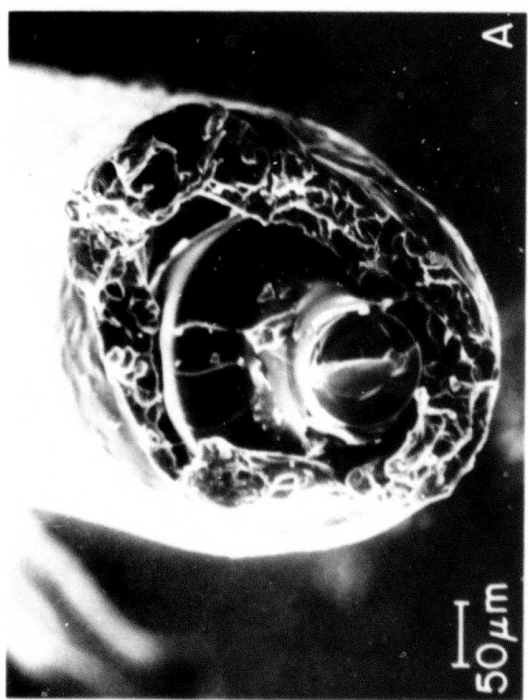
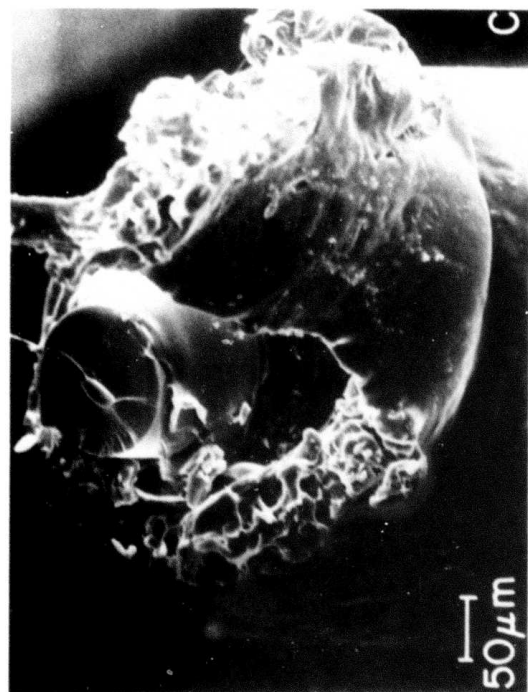


Fig. 16. SEM fractograph of an ITT fiber tested (at 3500 MN/m^2) at NOSC. A and B - 4-8; C and D- 2-6. These very large defects are unidentified, but would be expected to cause low strength ($< 700 \text{ MN/m}^2$) fractures. One would suspect, then, that these are probably secondary failures and do not reflect the primary break, or that the inhomogeneity is not a high stress concentration.



DISTRIBUTION LIST

Captain H. V. Winsor
DARPA/MSO
1400 Wilson Blvd.
Arlington, VA 22209

Dr. H. E. Rast
NOSC
San Diego, CA 92155

Dr. M. S. Maklad
ITT-EOPD
7635 Plantation Rd. 4253
Roanoke, VA 24019

Mr. C. Schleff
ITT-EOPD
7635 Plantation Rd.
Roanoke, VA 24019

Dr. D. A. Pinnow
Hughes Research Laboratory
3011 Malibu Canyon Rd.
Malibu, CA 90265

Mr. J. Wysocki
Hughes Research Laboratory
3011 Malibu Canyon Rd.
Malibu, CA 90265

Prof. P. B. Macedo
Vitreous State Laboratory
Keane Bldg.
Catholic University of America
Washington, D. C. 20017

Dr. K. M. Ferer
NORDA Code 351
NSTL
Bay St. Louis, MO 39520

Dr. J. Chalupka
Naval Sea Systems Command
NC-3
Arlington, VA 20362

Dr. G. H. Sigel
Code 6444
Naval Research Laboratory
Washington, D. C. 20375

Dr. F. W. Dabby
Times Fiber Communication, Inc.
359 Hall Ave.
Wallingford, CT 06492

Dr. L. L. Campbell
1662 Valencia Way
Reston, VA 22090

Dr. I. D. Aggarwal
Galileo Electro Optical Corp.
Galileo Park
Sturbridge, MA 01566

Dr. B. K. Teryial
Bell Laboratories
200 N.E. Expressway
Norcross, GA 30088

Dr. D. Kalish
Bell Telephone Laboratories
2000 N.E. Expressway
Norcross, GA 30071

Dr. C. J. Kurkjian
Bell Laboratories
Mountain Ave.
Murray Hill, NJ 07974

Dr. J. E. Ritter, Jr.
Univ. of Massachusetts
Mechanical Engineering Dept.
Amherst, MA 01002

Dr. G. K. Bansal
Battelle Columbus Laboratory
505 King Ave.
Columbus, OH 43201

Dr. A. M. Diness
Office of Naval Research
Code 471
800 N. Quincy St.
Arlington, VA 22217

Mr. C. Bersch
Naval Air Systems Command
Washington, D. C. 20361

Dr. W. E. Snowden
General Electric Company
Nela Park, OH 44102

Dr. R. D. Maurer
Corning Glass Works
Corning, NY 14830

Dr. Bernie Bendow
RADC/ET
Hanscom AFB, MA 01731

Mr. James F. Bacon
UTRC
E. Hartford, CT 06040